Tenth-order QED contribution to the lepton anomalous magnetic moment: Sixth-order vertices containing an internal light-by-light-scattering subdiagram

Tatsumi Aoyama, Masashi Hayakawa, Toichiro Kinoshita, and Makiko Nio

Phys. Rev. D **85**, 093013 — Published 21 May 2012
DOI: 10.1103/PhysRevD.85.093013

Tenth-Order QED Contribution to the Lepton Anomalous Magnetic Moment – Sixth-Order Vertices Containing an Internal Light-by-Light-Scattering Subdiagram

Tatsumi Aoyama,[1,2] Masashi Hayakawa,[3,2] Toichiro Kinoshita,[4,2] and Makiko Nio[2]

[1]*Kobayashi-Maskawa Institute for the Origin of Particles and the Universe (KMI), Nagoya University, Nagoya, 464-8602, Japan*

[2]*Nishina Center, RIKEN, Wako, 351-0198, Japan*

[3]*Department of Physics, Nagoya University, Nagoya, Japan 464-8602*

[4]*Laboratory for Elementary-Particle Physics, Cornell University, Ithaca, New York, 14853, U.S.A*

Abstract

This paper reports the tenth-order QED contribution to the lepton g–2 from the gauge-invariant set, called Set III(c), which consists of 390 Feynman vertex diagrams containing an internal fourth-order light-by-light-scattering subdiagram. The mass-independent contribution of Set III(c) to the electron $g-2$ (a_e) is 4.9210 (103) in units of $(\alpha/\pi)^5$. The mass-dependent contributions to a_e from diagrams containing a muon loop is 0.00370 (37) $(\alpha/\pi)^5$. The tau-lepton loop contribution is negligible at present. Altogether the contribution of Set III(c) to a_e is 4.9247 (104) $(\alpha/\pi)^5$. We have also evaluated the contribution of the closed electron loop to the muon $g-2$ (a_μ). The result is 7.435 (134) $(\alpha/\pi)^5$. The contribution of the tau-lepton loop to a_μ is 0.1999 (28) $(\alpha/\pi)^5$. The total contribution of various leptonic loops (electron, muon, and tau-lepton) of Set III(c) to a_μ is 12.556 (135) $(\alpha/\pi)^5$.

PACS numbers: 13.40.Em, 06.20.Jr,12.20.Ds,14.60.Cd

I. INTRODUCTION

The anomalous magnetic moment $a_e \equiv (g–2)/2$ of the electron has played the central role in testing the validity of quantum electrodynamics (QED) as well as the Standard Model. On the experimental side, the latest measurement of a_e by the Harvard group has reached the precision of 0.24×10^{-9} [1, 2]:

$$a_e(\text{HV08}) = 1\ 159\ 652\ 180.73\ (0.28) \times 10^{-12} \quad [0.24\text{ppb}]\ . \tag{1}$$

The theoretical prediction thus far consists of QED corrections of up to the eighth order [3–5], direct evaluation of hadronic corrections [6–12], and electroweak corrections scaled down from their contributions to the muon $g-2$ [13–15]. To compare the theory with the measurement (1), we also need the value of the fine structure constant α determined by a method independent of $g-2$. The best value of such an α available at present is one obtained from the measurement of h/m_{Rb}, the ratio of the Planck constant and the mass of Rb atom, combined with the very precisely known values of the Rydberg constant and m_{Rb}/m_e: [16]

$$\alpha^{-1}(\text{Rb10}) = 137.035\ 999\ 037\ (91) \quad [0.66\text{ppb}]. \tag{2}$$

With this α the theoretical prediction of a_e becomes

$$a_e(\text{theory}) = 1\ 159\ 652\ 181.13\ (0.11)(0.37)(0.02)(0.77) \times 10^{-12}, \tag{3}$$

where the first, second, third, and fourth uncertainties come from the calculated eighth-order QED term [5], the crude tenth-order estimate [17], the hadronic and electroweak contributions, and the fine structure constant (2), respectively. The theory (3) is in good agreement with the experiment (1):

$$a_e(\text{HV08}) - a_e(\text{theory}) = -0.40\ (0.88) \times 10^{-12}, \tag{4}$$

proving that QED (Standard Model) is in good shape even at this very high precision.

Eq. (3) shows clearly that the largest source of uncertainty is the fine structure constant (2). To put it differently, a non-QED α, even the best one available at present, is too crude to test QED to the extent achieved by the theory and measurement of a_e. Thus it makes more sense to test QED by an alternate approach, namely, obtain α from theory and measurement of a_e[1]:

$$\alpha^{-1}(a_e 08) = 137.035\ 999\ 085\ (12)(37)(2)(33) \quad [0.37\text{ppb}], \tag{5}$$

where the first, second, third, and fourth uncertainties come from the calculated eighth-order QED term, the crude tenth-order estimate, the hadronic and electroweak contributions, and the measurement of a_e(HV08), respectively.

Although the uncertainty of $\alpha^{-1}(a_e 08)$ in (5) is a factor 2 smaller than α^{-1}(Rb10), it is not a firm factor since it depends on the estimate of the tenth-order term, which is only a crude guess [17]. For a more stringent test of QED, it is obviously necessary to calculate the actual value of the tenth-order term. To meet this challenge we launched several years ago a systematic program to evaluate the complete tenth-order term [18–20].

The 10th-order QED contribution to the anomalous magnetic moment of an electron can be written as

$$a_e^{(10)} = \left(\frac{\alpha}{\pi}\right)^5 \left[A_1^{(10)} + A_2^{(10)}(m_e/m_\mu) + A_2^{(10)}(m_e/m_\tau) + A_3^{(10)}(m_e/m_\mu, m_e/m_\tau)\right], \tag{6}$$

where $m_e/m_\mu = 4.836\ 331\ 66\ (12) \times 10^{-3}$ and $m_e/m_\tau = 2.875\ 64\ (47) \times 10^{-4}$ [17]. In the rest of this article the factor $\left(\frac{\alpha}{\pi}\right)^5$ is suppressed for simplicity.

The diagrams contributing to the mass-independent term $A_1^{(10)}$ can be classified into six gauge-invariant sets, further divided into 32 gauge-invariant subsets depending on the nature of closed lepton loop subdiagrams. Thus far, numerical results of 30 gauge-invariant subsets, which consist of 5928 vertex diagrams, have been published [3, 21–27], or submitted for publication [28]. Five of these 30 subsets are also known analytically [29, 30]. They are in good agreement with our calculations.

In this paper we report the contribution to $A_1^{(10)}$ from the gauge-invariant subset called Set III(c), which consists of 390 vertex diagrams and is represented by 24 self-energy-like diagrams of Figure 1. A characteristic feature of these diagrams is that they have vertex and self-energy subdiagrams which contain a light-by-light (l-l) scattering subdiagram. They can be classified into three types:

1. Sixth-order vertex subdiagrams containing an l-l loop *externally* as is shown in Figure 2. Here "external" means that one of the photons is external to the subdiagrams containing the l-l loop.

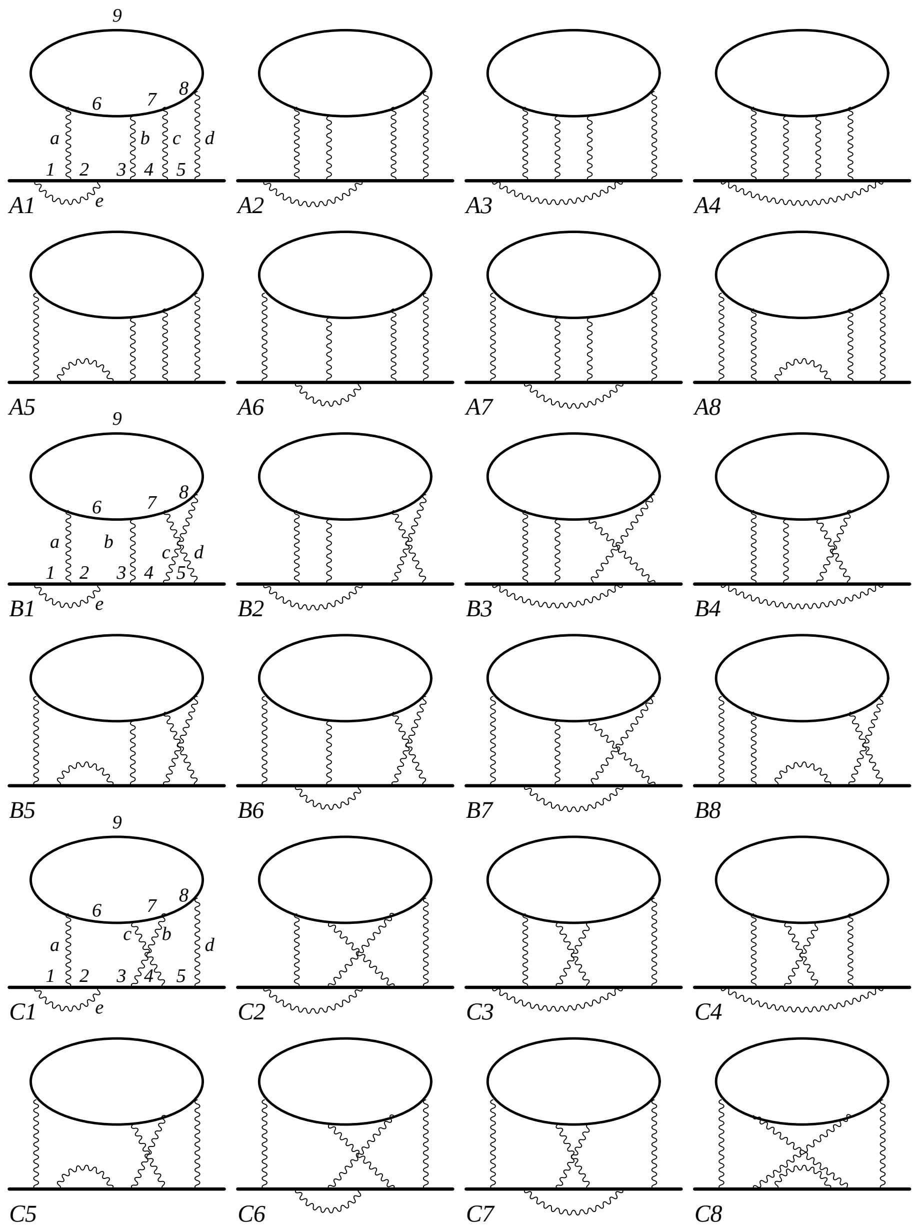

FIG. 1: Tenth-order self-energy-like diagrams in which lepton lines propagate in the magnetic field. They represent 390 vertex diagrams of Set III(c). Assignment of Feynman parameters $z_1, z_2, \ldots, z_9$ to the lepton lines and $z_a, z_b, .., z_e$ to the photon lines is indicated in the figure $A1$, $B1$, and $C1$.

2. Eighth-order vertex subdiagrams containing an l-l loop externally as is shown in Figure 3. They are obtained by applying a virtual photon correction on the open fermion line of a sixth-order l-l vertex subdiagram of Figure 2.

3. Eighth-order vertex and self-energy subdiagrams which contain an l-l loop internally.

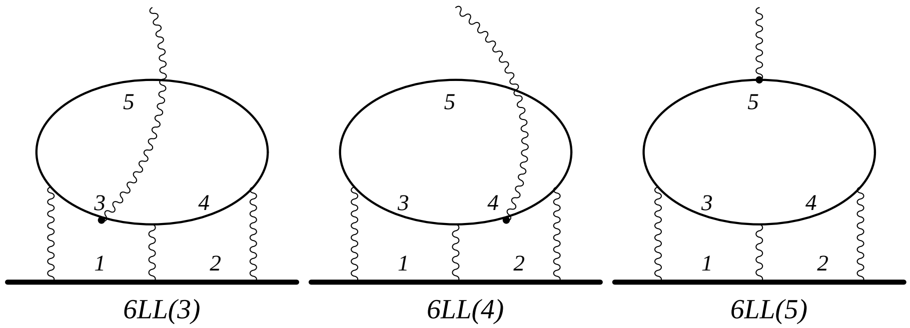

FIG. 2: Vertex diagrams of sixth order containing an l-l subdiagram. The diagram $6LL(3)$ and $6LL(4)$ are identical with each other because of the time-reversal symmetry. There are six vertex diagrams of this type, taking into account of two directions in which the closed fermion loop can take.

This type appears for the first time in the tenth-order perturbation theory of QED. See Figure 4.

The vertex subdiagrams of type 1 and type 2 do not have their Ward-Takahashi-related self-energy subdiagrams which vanish identically due to Furry's theorem. Thus, the gauge-invariant sums of the vertex renormalization constants of these external l-l subdiagrams also vanish identically.

For vertex subdiagrams of type 3, the corresponding self-energy subdiagrams do exist which have an internal l-l diagram. In this case both vertex subdiagram and self-energy subdiagram have UV divergence due to the sixth-order external l-l vertex subdiagram.

Because of these specific features of an l-l scattering diagram and vertex diagrams containing an external l-l loop, we adopt for the Set III(c) an approach different from the one used for a diagram without an l-l loop [19, 20]. Our formulation and treatment of UV divergences and IR divergences due to subdiagrams are described in Sec. II. Results of numerical evaluation will be presented in Sec. III. Sec. IV is devoted to the summary and discussion of this work. Renormalization of these diagrams is described in Appendix A.

II. FORMULATION

Instead of dealing with the 390 vertex diagrams of Set III(c) individually, we consider the sum Λ^ν of a set of vertex diagrams that are obtained from a self-energy-like diagram

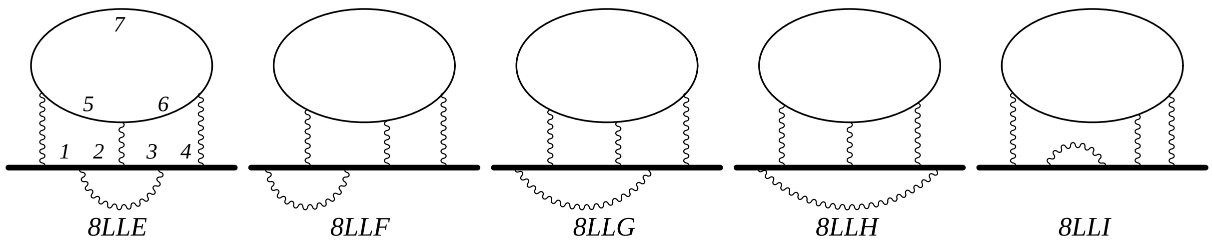

FIG. 3: Various diagrams of the eighth order needed for renormalization. $8LL\alpha$ ($\alpha = E, F, G, H, I$) is denoted as $LL\alpha$ in Ref. [31]. A vertex diagram $8LL\alpha(i)$ ($i = 5, 6, 7$) is obtained by inserting an external vertex into a fermion line i of the diagram $8LL\alpha$. It is denoted as $LL\alpha(i)$ in Ref. [32].

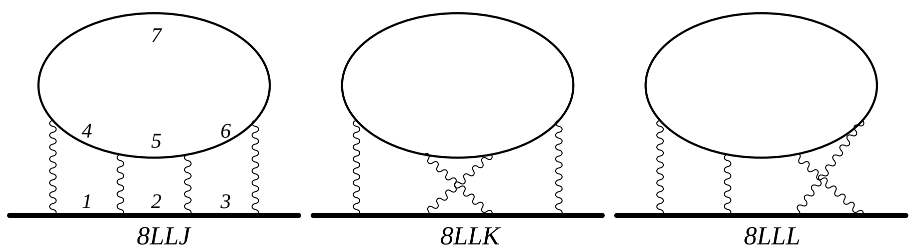

FIG. 4: The eighth-order self-energy-like diagrams $8LLJ$, $8LLK$, and $8LLL$, containing a light-by-light scattering loop internally. Open lepton lines propagate in the weak magnetic field. They represent 18 vertex diagrams in total. The vertex diagram $8LLJ(1)$ is a part of the diagram $8LLJ$ in which the magnetic vertex is attached only to the fermion line 1 of the self-energy diagram $8LLJ$.

$\Sigma(p)$ of Figure 1 by inserting a magnetic vertex γ^ν in the lepton lines 1, 2, 3, 4, and 5. We rewrite this Λ^ν as

$$\Lambda^\nu(p,q) \simeq -q^\mu \left[\frac{\partial \Lambda_\mu(p,q)}{\partial q_\nu}\right]_{q=0} - \frac{\partial \Sigma(p)}{\partial p_\nu}. \tag{7}$$

with the help of the Ward-Takahashi identity, where $p-q/2$ and $p+q/2$ are the 4-momenta of incoming and outgoing lepton lines and $(p-q/2)^2 = (p+q/2)^2 = m^2$. Each sum corresponds to one of the 24 self-energy-like diagrams shown in Figure 1. The $g-2$ term is projected out from the right-hand side of (7).

A. Construction of Unrenormalized Integrals

Each diagram $\mathcal{G}$ of Figure 1 can be expressed by a momentum integral applying the Feynman-Dyson rule. Introducing Feynman parameters $z_1, z_2, \ldots, z_9$ for the electron propagators and $z_a, z_b, \ldots, z_e$ for the photon propagators (see the figures A_1, B_1, and C_1 of Figure 1), we carry out the momentum integration analytically by means of a home-made program written in FORM [33]. This leads to an integral of the form

$$M_{\mathcal{G}} = -\left(\frac{-1}{4}\right)^5 4! \int (dz)_{\mathcal{G}} \left[\frac{1}{4}\left(\frac{E_0+C_0}{U^2V^4} + \frac{E_1+C_1}{U^3V^3} + \cdots\right) + \left(\frac{N_0+Z_0}{U^2V^5} + \frac{N_1+Z_1}{U^3V^4} + \cdots\right)\right], \tag{8}$$

where E_n, C_n, N_n and Z_n are functions of Feynman parameters, and "symbolic" building blocks A_i, B_{ij}, C_{ij}, for $i, j = 1, 2, \ldots, 9$. n is the number of contractions (see [34] for definitions). U is the Jacobian of transformation from the momentum space variables to Feynman parameters. A_i is the *scalar current* defined by

$$A_i = \eta_i - \frac{1}{U}\sum_{j=1}^{5} z_j B_{ij}, \qquad \begin{cases} \eta_i = 1 \text{ for } i = 1,2,3,4,5 \\ \eta_i = 0 \text{ for } i = 6,7,8,9 \end{cases}, \tag{9}$$

and

$$(dz)_{\mathcal{G}} = \prod_{i \in \mathcal{G}} dz_i (1 - \sum_{i \in \mathcal{G}} z_i). \tag{10}$$

B_{ij} is a Feynman-parameter translation of a bilinear form of the diagonalized loop momenta flowing in the fermion lines i and j and is determined by the topology of a given diagram. C_{ij} is defined from the first term of Eq. (7) through the operation that inserts an external vertex into a fermion line of a self-energy diagram. See, for example, Ref. [19] for exact definitions of B_{ij} and C_{ij}. V is obtained by combining all denominators of propagators into one with the help of Feynman parameters. It has a form common to all diagrams of Figure 1:

$$V = \sum_{i=1}^{9} z_i(1 - A_i)m_i^2 + \sum_{k=a}^{e} z_k \lambda_k^2, \tag{11}$$

where m_i and λ_k are the rest masses of lepton i and photon k, respectively. Of course, m_i is independent of i and λ_k is 0 independent of k. But it is useful to distinguish different lepton lines and photon lines in deriving Eq. (8). The form of A_i as a function of Feynman parameters depends on the structure of individual diagram $\mathcal{G}$ of Figure 1.

B. Renormalization

The diagrams of Set III(c) as a whole form a (formal) gauge-invariant set. However, individual diagrams have UV divergences arising from the light-by-light-scattering (l-l) subdiagram as well as vertex subdiagrams or self-energy subdiagrams. All these divergences must be regularized in advance. In order to maintain gauge invariance the l-l subdiagram may be regularized by the Pauli-Villars method or by the dimensional regularization. The sixth-order vertex renormalization constant associated with the diagram containing an l-l subdiagram and the eighth-order vertex renormalization constant containing an l-l subdiagram are logarithmically divergent, but their sum over all diagrams vanishes due to Ward-Takahashi identity. Note that the self-energy diagrams associated with these vertex diagrams do not exist in QED because of the Furry's theorem.

As is indicated in the figures $A1$, $B1$, $C1$ of Figure 1, we denote open fermion lines as 1, 2, 3, 4, 5, fermion lines forming a closed loop as 6, 7, 8, 9, and photon lines as a, b, c, d, e. We will identify a subdiagram containing open lepton lines in terms of a subset of (1,2,3,4,5). For instance, the vertex subdiagram (1,2) of $A1$ will be denoted by (1,2), and the vertex subdiagram {2,3,4,5; 6,7,8,9; b,c,d} of $A1$ will be denoted by (2,3,4,5). An exception is the l-l subdiagram, which will be denoted as (6,7,8,9). Under this convention the diagram $A1$ has five divergent subdiagrams $(1,2)$, $(4,5)$, $(1,2,3,4)$, $(2,3,4,5)$, and $(6,7,8,9)$. The fifteen UV subtraction terms can be constructed from these subdiagrams following the Zimmermann's forest formula [35].

Diagrammatically, the second-order vertex subdiagram appears not only in the forests including the subdiagram $(1,2)$ but also in the forest $(2,3,4,5)(4,5)$. In the latter, the reduced diagram $(2,3)$ forms a second-order vertex diagram. We will treat renormalization of this *implicit* second-order vertex in a manner different from the *explicit* second-order vertex. A detailed account will be given in Appendix A.

The UV divergence arising from the explicit second-order vertex (1,2) of the diagram $A1$ can be subtracted by an integral defined by the K_{12}-operation [34] applied on the integral M_{A1}. The K_{12}-operation is defined in such a way that the result of the operation factorizes exactly as

$$K_{12}M_{A1} = L_2^{(1,2)UV} M_{8LLJ}^{(3,4,5)}, \tag{12}$$

where $L_2^{(1,2)UV}$ is the UV-divergent part of the second-order on-shell vertex renormalization constant $L_2^{(1,2)}$ and $M_{8LLJ}^{(3,4,5)}$ is the magnetic moment amplitude from the eighth-order self-energy-like diagram $8LLJ$ of Figure 4.

UV divergences from the explicit second-order vertex subdiagram are also found in the diagrams $B1, C1, A6, B6$, and $C6$. UV divergences due to the explicit second-order self-energy-like subdiagram come from the diagrams $A5, B5, C5, A8, B8$, and $C8$. The renormalization scheme in which only these second-order divergences appear are handled by the K-operation and is described in Appendix A.

All other subdiagrams contain an l-l subdiagram, which we treat by the Pauli-Villars method or by the dimensional regularization. For instance, in the latter method, let $F_{\alpha i}(d)$ be one of such integrals defined in d dimension, where αi takes values $\alpha = A, B, C;\ i = 1, 2, ..., 8$. Let $G_{\alpha i}(d)$ be $F_{\alpha i}(d)$ in which the l-l subdiagram (of the form $\Pi_{\mu\nu\sigma\rho}(k_1, k_2, k_3, k_4)$) is replaced by the tensor with zero external momenta, namely, $\Pi_{\mu\nu\sigma\rho}(0, 0, 0, 0)$. Let us rewrite $F_{\alpha i}(d)$ symbolically as

$$[F_{\alpha i}(d) - G_{\alpha i}(d)] + G_{\alpha i}(d), \tag{13}$$

where by "symbolically" we mean that subtraction is performed on the integrand before the integration is carried out. Now we can safely take the limit $d \to 4$ for the term $[F_{\alpha i}(d) - G_{\alpha i}(d)]$ since its integrand does not cause UV divergence. Of course, the second term $G_{\alpha i}(d)$ is singular for $d \to 4$. However, gauge invariance guarantees that the sum of $G_{\alpha i}(d)$ over all diagrams of Figure 1 vanishes for any value of dimension d:

$$\sum_{\alpha=A}^{C} \sum_{i=1}^{8} \eta_i G_{\alpha i}(d) = 0, \tag{14}$$

where $\eta_i = 2$ for $i = 4, 7, 8$, and $\eta_i = 4$ for $i = 1, 2, 3, 5, 6$. Thus, in the end, we have to compute only

$$\lim_{d \to 4} [F_{\alpha i}(d) - G_{\alpha i}(d)]. \tag{15}$$

Of course the same result is obtained by the Pauli-Villars method. To avoid crowded notations let us use $F_{\alpha i}(4)$ instead of Eq. (15) in the following.

Each self-energy-like diagram of Figure 1 represents the sum of five vertex diagrams. Diagrams obtained by reversing the momentum flow within the l-l loop are not shown but they give the same integrals as the original ones. Another factor 2 must be included for diagrams that are not symmetric under time-reversal. Thus, integrals for diagrams such as $A1$ actually represent $2 \times 2 \times 5$ vertex diagrams. The $g-2$ contribution from the sum of all diagrams of Set III(c), after the renormalization described in Appendix A is carried out, can thus be written as

$$A_1^{(10)}[\text{Set III(c)}^{(l_1 l_2)}] = \sum_{\alpha=A}^{C} \sum_{i=1}^{8} \eta_i \Delta M_{\alpha i}^{(l_1 l_2)} - 3 \Delta LB_2 \Delta M_{8JKL}^{(l_1 l_2)}, \tag{16}$$

where $\Delta M_{\alpha i}^{(l_1 l_2)}$ is the finite ampitude of the diagram αi, $\alpha = A, B, C$, and $i = 1, 2, \cdots, 8$ defined in Appendix A. The superscripts l_1 refers to the open lepton line and l_2 refers to the closed lepton line. $\eta_i = 2$ for $i = 4, 7, 8$, and $\eta_i = 4$ for $i = 1, 2, 3, 5, 6$. ΔLB_2 and $\Delta M_{8JKL}^{(l_1 l_2)}$ are defined in Appendix A.

III. NUMERICAL RESULTS

Evaluation of integral $\Delta M_{\alpha i}^{(l_1 l_2)}$ is carried out by the adaptive-iterative Monte-Carlo integration routine VEGAS [36]. The results for the case $(l_1 l_2) = (ee)$ are listed in Table I. From this table and Table II listing the residual renormalization terms we obtain

$$A_1^{(10)}[\text{Set III(c)}^{(ee)}] = 4.9210\ (103). \tag{17}$$

The contribution of the muon loop to a_e can be calculated from the data listed in Table III and Table II:

$$A_2^{(10)}[\text{Set III(c)}^{(em)}] = 0.00370\ (37). \tag{18}$$

The contribution of the tau-lepton loop to a_e is within the uncertainty of (17). Thus the total QED contribution to $a_e^{(10)}$ is essentially the sum of (17) and (18):

$$a_e^{(10)}[\text{Set III(c)}] = 4.9247\ (104) \left(\frac{\alpha}{\pi}\right)^5. \tag{19}$$

FORTRAN programs for a_e can be readily adapted to the evaluation of a_μ. The results of evaluation of the contribution of the electron loop to the muon $g-2$ are listed in Table IV. From this table and Table II we obtain

$$A_2^{(10)}[\text{Set III(c)}^{(me)}] = 7.435\ (134). \tag{20}$$

The contribution of the tau-lepton loop to a_μ is calculated from the data listed in Table V and Table II:

$$A_2^{(10)}[\text{Set III(c)}^{(mt)}] = 0.1999\ (28). \tag{21}$$

The total QED contribution to $a_\mu^{(10)}$ is the sum of (17), (20), and (21):

$$a_\mu^{(10)}[\text{Set III(c)}] = 12.556\ (135) \left(\frac{\alpha}{\pi}\right)^5. \tag{22}$$

TABLE I: Contributions of diagrams of Set III(c) to a_e for $(l_1 l_2) = (ee)$ obtained by VEGAS at RICC. The superscript (ee) is suppressed for simplicity. The multiplicity n_F is the number of vertex diagrams represented by the integral and is incorporated in the numerical value. All integrals are evaluated initially with 10^8 sampling points per iteration, iterated 50 times, followed by 10^9 points, iterated several times.

Integral	n_F	Value (Error) including n_F	Sampling per iteration	No. of iterations
ΔM_{A1}	20	$-4.255\ 92\ (253)$	$1 \times 10^8,\ 1 \times 10^9$	50, 400
ΔM_{A2}	20	$4.938\ 78\ (244)$	$1 \times 10^8,\ 1 \times 10^9$	50, 300
ΔM_{A3}	20	$-1.546\ 88\ (246)$	$1 \times 10^8,\ 1 \times 10^9$	50, 345
ΔM_{A4}	10	$-0.323\ 88\ (127)$	$1 \times 10^8,\ 1 \times 10^9$	50, 30
ΔM_{A5}	20	$6.320\ 29\ (153)$	$1 \times 10^8,\ 1 \times 10^9$	50, 60
ΔM_{A6}	20	$-5.660\ 33\ (218)$	$1 \times 10^8,\ 1 \times 10^9$	50, 300
ΔM_{A7}	10	$2.284\ 61\ (173)$	$1 \times 10^8,\ 1 \times 10^9$	50, 65
ΔM_{A8}	10	$1.362\ 06\ (129)$	$1 \times 10^8,\ 1 \times 10^9$	50, 20
ΔM_{B1}	20	$5.693\ 53\ (293)$	$1 \times 10^8,\ 1 \times 10^9$	50, 412
ΔM_{B2}	20	$-7.018\ 17\ (273)$	$1 \times 10^8,\ 1 \times 10^9$	50, 302
ΔM_{B3}	20	$3.735\ 46\ (260)$	$1 \times 10^8,\ 1 \times 10^9$	50, 342
ΔM_{B4}	10	$-0.052\ 76\ (122)$	$1 \times 10^8,\ 1 \times 10^9$	50, 30
ΔM_{B5}	20	$-4.739\ 40\ (166)$	$1 \times 10^8,\ 1 \times 10^9$	50, 60
ΔM_{B6}	20	$3.061\ 01\ (212)$	$1 \times 10^8,\ 1 \times 10^9$	50, 300
ΔM_{B7}	10	$0.351\ 39\ (168)$	$1 \times 10^8,\ 1 \times 10^9$	50, 65
ΔM_{B8}	10	$-0.793\ 52\ (136)$	$1 \times 10^8,\ 1 \times 10^9$	50, 20
ΔM_{C1}	20	$0.377\ 40\ (279)$	$1 \times 10^8,\ 1 \times 10^9$	50, 417
ΔM_{C2}	20	$3.054\ 41\ (241)$	$1 \times 10^8,\ 1 \times 10^9$	50, 300
ΔM_{C3}	20	$-1.329\ 04\ (260)$	$1 \times 10^8,\ 1 \times 10^9$	50, 338
ΔM_{C4}	10	$0.435\ 88\ (131)$	$1 \times 10^8,\ 1 \times 10^9$	50, 30
ΔM_{C5}	20	$-3.729\ 22\ (159)$	$1 \times 10^8,\ 1 \times 10^9$	50, 60
ΔM_{C6}	20	$4.273\ 41\ (258)$	$1 \times 10^8,\ 1 \times 10^9$	50, 300
ΔM_{C7}	10	$-2.233\ 00\ (159)$	$1 \times 10^8,\ 1 \times 10^9$	50, 65
ΔM_{C8}	10	$-1.514\ 28\ (142)$	$1 \times 10^8,\ 1 \times 10^9$	50, 20

IV. DISCUSSION

All programs of diagrams of the Set III(c) were written in two independent ways, in order to detect possible programming error. No such error was found.

The value of $A_2^{(10)}[\text{Set III(c)}^{(me)}]$ given in (20) is not much larger than that of $A_1^{(10)}[\text{Set III(c)}^{(ee)}]$ given in (17). This is somewhat unexpected since, as is seen from Table IV, individual integrals contributing to $A_2^{(10)}[\text{Set III(c)}^{(me)}]$ are an order of magnitude larger than those given in Table I. Presumably, the modest value of (20) is a consequence of strong cancellation among contributing integrals.

TABLE II: Auxiliary integrals for Set III(c). Some integrals are known exactly. Other integrals are obtained by the integration routine VEGAS. The superscript ($l_1\ l_2$) indicates that the open and closed fermion lines consist of fermions l_1 and l_2, respectively. The letters e, m, and t stand for electron, muon, and tau-lepton, respectively.

Integral	Value (error)	Integral	Value (error)
M_2	0.5	ΔLB_2	0.75
$\Delta M_{8JKL}^{(ee)}$	−0.990 72 (11)	$\Delta M_{8JKL}^{(me)}$	−4.432 43 (59)
$\Delta M_{8JKL}^{(em)}$	−0.000 177 8 (13)	$\Delta M_{8JKL}^{(mt)}$	−0.015 87 (5)

Acknowledgments

We thank Mr. N. Watanabe for his contribution in the early stage of this work. This work is supported in part by the JSPS Grant-in-Aid for Scientific Research (C)19540322, (C)20540261, and (C)23540331. The part of material presented by T. K. is based on work supported by the U. S. National Science Foundation under the Grant NSF-PHY-0757868, and the International Exchange Support Grants (FY2010) of RIKEN. T. K. thanks RIKEN for the hospitality extended to him while a part of this work was carried out. Numerical calculations are conducted on the RIKEN Supercombined Cluster System (RSCC), the RIKEN Integrated Cluster of Clusters (RICC) supercomputing systems, and the φ computer of Kobayashi-Maskawa Institute. A part of preliminary computations was also conducted on the computers of the theoretical particle-physics group (E-ken), Nagoya University.

Appendix A: Renormalization of diagrams of Set III(c)

Diagrams of Set III(c), shown in Figure 1, contain an l-l subdiagram internally. Thus we find it convenient to pursue a renormalization scheme somewhat different from all other Sets contributing to the tenth-order $g-2$. As is indicated by figures $A1$, $B1$, $C1$ of Figure 1, we denote open fermion lines as 1, 2, 3, 4, 5, closed fermion lines as 6, 7, 8, 9, and photon lines as a, b, c, d, e. We will identify a subdiagram containing open lepton lines in terms of their line numbers. For instance, the second-order vertex subdiagram {1,2;e} and sixth-order vertex subdiagram {4,5;6,7,8,9;b,c,d} of $A1$ will be denoted by the superscript (1,2) and

TABLE III: Contributions of diagrams of Set III(c) to a_e for $(l_1 l_2) = (em)$ obtained by VEGAS at RICC. The superscript (em) is suppressed for simplicity. The multiplicity n_F is the number of vertex diagrams represented by the integral and is incorporated in the numerical value. All integrals are evaluated with 10^7 sampling points per iteration, iterated 50 times, and subsequently evaluated with 10^8 sampling points per iteration, iterated 50 times.

Integral	n_F	Value (Error) including n_F	Sampling per iteration	No. of iterations
ΔM_{A1}	20	$-0.016\ 78\ (15)$	$1\times 10^7,\ 1\times 10^8$	50, 50
ΔM_{A2}	20	$-0.004\ 71\ (8)$	$1\times 10^7,\ 1\times 10^8$	50, 50
ΔM_{A3}	20	$0.000\ 99\ (6)$	$1\times 10^7,\ 1\times 10^8$	50, 50
ΔM_{A4}	10	$-0.003\ 93\ (1)$	$1\times 10^7,\ 1\times 10^8$	50, 50
ΔM_{A5}	20	$0.007\ 01\ (1)$	$1\times 10^7,\ 1\times 10^8$	50, 50
ΔM_{A6}	20	$-0.023\ 43\ (12)$	$1\times 10^7,\ 1\times 10^8$	50, 50
ΔM_{A7}	10	$-0.001\ 00\ (2)$	$1\times 10^7,\ 1\times 10^8$	50, 50
ΔM_{A8}	10	$0.001\ 97\ (1)$	$1\times 10^7,\ 1\times 10^8$	50, 50
ΔM_{B1}	20	$0.007\ 61\ (15)$	$1\times 10^7,\ 1\times 10^8$	50, 50
ΔM_{B2}	20	$0.000\ 37\ (8)$	$1\times 10^7,\ 1\times 10^8$	50, 50
ΔM_{B3}	20	$0.000\ 46\ (4)$	$1\times 10^7,\ 1\times 10^8$	50, 50
ΔM_{B4}	10	$0.003\ 05\ (1)$	$1\times 10^7,\ 1\times 10^8$	50, 50
ΔM_{B5}	20	$0.010\ 68\ (1)$	$1\times 10^7,\ 1\times 10^8$	50, 50
ΔM_{B6}	20	$0.015\ 17\ (11)$	$1\times 10^7,\ 1\times 10^8$	50, 50
ΔM_{B7}	10	$0.002\ 24\ (2)$	$1\times 10^7,\ 1\times 10^8$	50, 50
ΔM_{B8}	10	$-0.013\ 72\ (1)$	$1\times 10^7,\ 1\times 10^8$	50, 50
ΔM_{C1}	20	$0.010\ 57\ (12)$	$1\times 10^7,\ 1\times 10^8$	50, 50
ΔM_{C2}	20	$0.004\ 88\ (5)$	$1\times 10^7,\ 1\times 10^8$	50, 50
ΔM_{C3}	20	$0.000\ 87\ (4)$	$1\times 10^7,\ 1\times 10^8$	50, 50
ΔM_{C4}	10	$0.000\ 84\ (1)$	$1\times 10^7,\ 1\times 10^8$	50, 50
ΔM_{C5}	20	$-0.018\ 16\ (1)$	$1\times 10^7,\ 1\times 10^8$	50, 50
ΔM_{C6}	20	$0.009\ 57\ (10)$	$1\times 10^7,\ 1\times 10^8$	50, 50
ΔM_{C7}	10	$0.000\ 93\ (2)$	$1\times 10^7,\ 1\times 10^8$	50, 50
ΔM_{C8}	10	$0.011\ 40\ (1)$	$1\times 10^7,\ 1\times 10^8$	50, 50

(4,5), respectively. An exception is the l-l subdiagram, which will be denoted as (6,7,8,9). Of course this is just for the sake of keeping track of where a particular subdiagram is located. The superscript will be removed when it is no longer needed.

1. *A1, B1, C1*

Let us begin with the g–2 amplitude M_{A1}. Noting that, out of 15 forests of the diagram $A1$ mentioned in Sec. II B, 8 are hidden in our convention leading to Eq. (15), the renormalized

TABLE IV: Contributions of diagrams of Set III(c) to a_μ for $(l_1 l_2) = (me)$ obtained by VEGAS at RICC. The superscript (me) is suppressed for simplicity. The multiplicity n_F is the number of vertex diagrams represented by the integral and is incorporated in the numerical value. All integrals are evaluated initially with 10^8 sampling points per iteration, iterated 50 times, followed by 10^9 points, iterated several times.

Integral	n_F	Value (Error) including n_F	Sampling per iteration	No. of iterations
ΔM_{A1}	20	-18.722 (37)	$1\times10^8,\ 1\times10^9$	50, 376
ΔM_{A2}	20	40.155 (26)	$1\times10^8,\ 1\times10^9$	50, 300
ΔM_{A3}	20	-3.780 (36)	$1\times10^8,\ 1\times10^9$	50, 366
ΔM_{A4}	10	-18.309 (11)	$1\times10^8,\ 1\times10^9$	50, 30
ΔM_{A5}	20	9.416 (14)	$1\times10^8,\ 1\times10^9$	50, 80
ΔM_{A6}	20	-37.911 (30)	$1\times10^8,\ 1\times10^9$	50, 301
ΔM_{A7}	10	19.431 (16)	$1\times10^8,\ 1\times10^9$	50, 85
ΔM_{A8}	10	10.371 (7)	$1\times10^8,\ 1\times10^9$	50, 70
ΔM_{B1}	20	54.402 (38)	$1\times10^8,\ 1\times10^9$	50, 471
ΔM_{B2}	20	-73.374 (29)	$1\times10^8,\ 1\times10^9$	50, 300
ΔM_{B3}	20	29.954 (38)	$1\times10^8,\ 1\times10^9$	50, 382
ΔM_{B4}	10	2.578 (13)	$1\times10^8,\ 1\times10^9$	50, 30
ΔM_{B5}	20	-49.408 (20)	$1\times10^8,\ 1\times10^9$	50, 80
ΔM_{B6}	20	-1.509 (33)	$1\times10^8,\ 1\times10^9$	50, 301
ΔM_{B7}	10	9.521 (20)	$1\times10^8,\ 1\times10^9$	50, 85
ΔM_{B8}	10	29.116 (9)	$1\times10^8,\ 1\times10^9$	50, 70
ΔM_{C1}	20	-31.212 (37)	$1\times10^8,\ 1\times10^9$	50, 497
ΔM_{C2}	20	36.233 (32)	$1\times10^8,\ 1\times10^9$	50, 300
ΔM_{C3}	20	-25.285 (37)	$1\times10^8,\ 1\times10^9$	50, 409
ΔM_{C4}	10	15.428 (16)	$1\times10^8,\ 1\times10^9$	50, 30
ΔM_{C5}	20	28.857 (22)	$1\times10^8,\ 1\times10^9$	50, 80
ΔM_{C6}	20	43.793 (38)	$1\times10^8,\ 1\times10^9$	50, 310
ΔM_{C7}	10	-27.637 (17)	$1\times10^8,\ 1\times10^9$	50, 85
ΔM_{C8}	10	-44.647 (11)	$1\times10^8,\ 1\times10^9$	50, 75

amplitude a_{A1} can be written as

$$\begin{aligned} a_{A1} \;=\; & M_{A1} - L_2^{(1,2)} M_{8LLJ}^{(3,4,5)} - L_{6LL(5)}^{(4,5)} M_{4a}^{(1,2,3)} - L_{8LLF(7)}^{(1,2,3,4)} M_2^{(5)} - L_{8LLJ(1)}^{(2,3,4,5)} M_2^{(1)} \\ & + \; L_2^{(1,2)} L_{6LL(5)}^{(4,5)} M_2^{(3)} + L_2^{(1,2)} L_{6LL(5)}^{(3,4)} M_2^{(5)} + L_2^{(2,3)} L_{6LL(5)}^{(4,5)} M_2^{(1)} . \end{aligned} \tag{A1}$$

As was discussed in Sec. II, all terms of (A1) containing an l-l subdiagram are to be understood as shorthands for the regularized quantity defined by Eq. (15). In other words, the UV divergence arising from the l-l subdiagram has been removed by the procedure described in Sec. II so that it can be treated as a UV-finite quantity. M_{8LLJ} is the proper magnetic moment amplitude of the eighth-order diagram $8LLJ$ of Figure 4. See [31, 32] for its precise

TABLE V: Contributions of diagrams of Set III(c) to a_μ for $(l_1l_2) = (mt)$ obtained by VEGAS at RICC. The superscript (mt) is suppressed for simplicity. The multiplicity n_F is the number of vertex diagrams represented by the integral and is incorporated in the numerical value. Most integrals are evaluated initially with 10^8 sampling points per iteration, iterated 50 times, followed by 10^9 points, iterated several times. ΔM_{A4}, ΔM_{B4}, ΔM_{C4}, and ΔM_{C8} are evaluated with 10^8 sampling points per iteration and iterated 50 times.

Integral	n_F	Value (Error) including n_F	Sampling per iteration	No. of iterations
ΔM_{A1}	20	−0.423 43 (111)	$1\times10^8,\ 1\times10^9$	50, 40
ΔM_{A2}	20	−0.001 66 (64)	$1\times10^8,\ 1\times10^9$	50, 30
ΔM_{A3}	20	0.033 30 (59)	$1\times10^8,\ 1\times10^9$	50, 30
ΔM_{A4}	10	−0.102 91 (13)	1×10^8	50
ΔM_{A5}	20	0.327 57 (14)	$1\times10^8,\ 1\times10^9$	50, 15
ΔM_{A6}	20	−0.600 58 (75)	$1\times10^8,\ 1\times10^9$	50, 40
ΔM_{A7}	10	0.011 26 (30)	$1\times10^8,\ 1\times10^9$	50, 15
ΔM_{A8}	10	0.065 01 (9)	$1\times10^8,\ 1\times10^9$	50, 15
ΔM_{B1}	20	0.246 29 (111)	$1\times10^8,\ 1\times10^9$	50, 40
ΔM_{B2}	20	−0.104 08 (64)	$1\times10^8,\ 1\times10^9$	50, 30
ΔM_{B3}	20	0.052 89 (49)	$1\times10^8,\ 1\times10^9$	50, 30
ΔM_{B4}	10	0.076 46 (11)	1×10^8	50
ΔM_{B5}	20	0.114 81 (13)	$1\times10^8,\ 1\times10^9$	50, 15
ΔM_{B6}	20	0.397 59 (67)	$1\times10^8,\ 1\times10^9$	50, 40
ΔM_{B7}	10	0.043 30 (25)	$1\times10^8,\ 1\times10^9$	50, 15
ΔM_{B8}	10	−0.298 83 (9)	$1\times10^8,\ 1\times10^9$	50, 15
ΔM_{C1}	20	0.251 61 (108)	$1\times10^8,\ 1\times10^9$	50, 40
ΔM_{C2}	20	0.137 58 (51)	$1\times10^8,\ 1\times10^9$	50, 30
ΔM_{C3}	20	−0.052 89 (51)	$1\times10^8,\ 1\times10^9$	50, 30
ΔM_{C4}	10	0.026 64 (10)	1×10^8	50
ΔM_{C5}	20	−0.476 30 (12)	$1\times10^8,\ 1\times10^9$	50, 15
ΔM_{C6}	20	0.268 81 (65)	$1\times10^8,\ 1\times10^9$	50, 40
ΔM_{C7}	10	−0.038 53 (25)	$1\times10^8,\ 1\times10^9$	50, 15
ΔM_{C8}	10	0.213 27 (14)	1×10^8	50

definition. L_2 is the vertex renormalization constant of the second order. $L_{6LL(5)}$ is the renormalization constant associated with the sixth-order vertex diagram $6LL(5)$ shown in Figure 2. $L_{8LLF(7)}$ and $L_{8LLJ(1)}$ are the eighth-order vertex renormalization constants associated with the self-energy-like diagrams $8LLF$ of Figure 3 and $8LLJ$ of Figure 4, respectively.

In the amplitude M_{A1}, the K-operation is applied only on the *explicit* second-order vertex subdiagram (1,2). For other terms the full bodies of the vertex renormalization constants of the sixth- and eighth-orders are used and subtracted. These vertex renormalization constants are extracted from a vertex diagram $\Gamma_\nu(p,q)$, where $(p-q/2)^2 = (p+q/2)^2 = m^2$, using the projection operator

$$L = \frac{1}{4}\mathrm{Tr}[(\not{p} + m)p^\nu \Gamma_\nu]|_{q=0} \ . \tag{A2}$$

The result is combined with the lower-order magnetic moment amplitude using, for instance, the factorization procedure described in Sec. III D of Ref. [19] backwards so that the combined formula is described by the same set of Feynman parameters as those of the unrenormalized magnetic moment M_{A1}. Then the UV-finite quantity ΔM_{A1} can be written as

$$\begin{aligned}\Delta M_{A1} &= M_{A1} - L_2^{UV(1,2)} M_{8LLJ}^{(3,4,5)} - L_{6LL(5)}^{(4,5)} M_{4a}^{(1,2,3)} - L_{8LLF(7)}^{(1,2,3,4)} M_2^{(5)} - L_{8LLJ(1)}^{(2,3,4,5)} M_2^{(1)} \\ &+ L_2^{UV(1,2)} L_{6LL(5)}^{(3,4)} M_2^{(5)} + L_2^{UV(1,2)} L_{6LL(5)}^{(4,5)} M_2^{(3)} + L_2^{(2,3)} L_{6LL(5)}^{(4,5)} M_2^{(1)}.\end{aligned} \tag{A3}$$

where $L_2^{UV(1,2)}$ is the UV-divergent part of $L_2^{(1,2)}$ defined by the K-operation. Note that $L_{6LL(5)}^{(3,4)}$, $L_{6LL(5)}^{(4,5)}$, $L_{8LLF(7)}^{(1,2,3,4)}$, $L_{8LLJ(1)}^{(2,3,4,5)}$, $L_2^{(2,3)}$, and $L_{6LL(5)}^{(4,5)}$ are not decomposed into UV-divergent and UV-finite parts. Note, in particular, that $L_2^{(2,3)}$ has an IR-divergent part besides a UV-divergent part. This is the reason why we normally avoid use of the whole L_2 as a subtraction term and use the L_2^{UV} defined by the K-operation instead. For the diagram $A1$, however, the IR divergences in $L_2^{(2,3)}$ and $L_{8LLJ(1)}$ cancel each other. Thus the UV-divergence-free amplitude ΔM_{A1} is also IR-divergence-free. The numerical integration code for the Set III(c) is constructed taking this observation into account.

Substituting (A3) in (A1) we obtain

$$\begin{aligned}a_{A1} &= \Delta M_{A1} - L_2^{\mathrm{R}} M_{8LLJ}^{(3,4,5)} + L_2^{\mathrm{R}} L_{6LL(5)}^{(3,4)} M_2 + L_2^{\mathrm{R}} L_{6LL(5)}^{(4,5)} M_2 \\ &= \Delta M_{A1} - L_2^{\mathrm{R}} \Delta M_{8LLJ},\end{aligned} \tag{A4}$$

where $L_2^{\mathrm{R}} \equiv L_2 - L_2^{UV}$ is UV-finite but IR-divergent and $\Delta M_{8LLJ} = M_{8LLJ} - 2L_{6LL(5)} M_2$ is the finite $g-2$ contribution from the eighth-order diagram $8LLJ$ [31, 32].

Similar consideration for the diagrams $B1$ and $C1$ yields

$$\begin{aligned}a_{B1} &= \Delta M_{B1} - L_2^{\mathrm{R}} M_{8LLL}^{(3,4,5)} + 2L_2^{\mathrm{R}} L_{6LL(3)} M_2 \\ &= \Delta M_{B1} - L_2^{\mathrm{R}} \Delta M_{8LLL},\end{aligned} \tag{A5}$$

and

$$\begin{aligned}a_{C1} &= \Delta M_{C1} - L_2^{\mathrm{R}} M_{8LLK}^{(3,4,5)} + 2L_2^{\mathrm{R}} L_{6LL(3)}^{(3,4)} M_2 \\ &= \Delta M_{C1} - L_2^{\mathrm{R}} \Delta M_{8LLK}.\end{aligned} \tag{A6}$$

From (A4), (A5), and (A6) we obtain

$$\sum_{\alpha=A}^{C} a_{\alpha 1} = \sum_{\alpha=A}^{C} \Delta M_{\alpha 1} - L_2^{\mathrm{R}} \Delta M_{8JKL}, \tag{A7}$$

where $\Delta M_{8JKL} \equiv \Delta M_{8LLJ} + \Delta M_{8LLK} + \Delta M_{8LLL}$ [31]. Note that the sum $L_{6LL} \equiv L_{6LL(3)} + L_{6LL(4)} + L_{6LL(5)} = 0$ because of the gauge invariance.

2. *A2, B2, C2*

The diagram $A2$ has UV-divergent subdiagrams $(1,2,3,4)$, $(2,3,4,5)$ besides the l-l subdiagram $(6,7,8,9)$. Thus the renormalized amplitude a_{A2} can be written as

$$a_{A2} = M_{A2} - M_2^{(1)} L_{8LLJ(2)}^{(2,3,4,5)} - L_{8LLG(7)}^{(1,2,3,4)} M_2^{(5)}. \tag{A8}$$

Diagrams $8LLJ$ and $8LLG$ are shown in Figure 3. Since $A2$ has no UV divergence due to the second-order subdiagram, we define ΔM_{A2} by

$$\Delta M_{A2} = M_{A2} - M_2^{(1)} L_{8LLJ(2)}^{(2,3,4,5)} - L_{8LLG(7)}^{(1,2,3,4)} M_2^{(5)}. \tag{A9}$$

Substituting (A9) in (A8) we obtain

$$a_{A2} = \Delta M_{A2}. \tag{A10}$$

Similar equations hold for a_{B2} and a_{C2}. Thus we have

$$\sum_{\alpha=A}^{C} a_{\alpha 2} = \sum_{\alpha=A}^{C} \Delta M_{\alpha 2}. \tag{A11}$$

3. *A3, B3, C3*

The diagram $A3$ has five forests after the l-l subdiagrams are treated following the consideration of Sec. II B. Thus the renormalized amplitude a_{A3} can be written as

$$\begin{aligned} a_{A3} \;=\; & M_{A3} - M_2^{(1)} L_{8LLJ(3)}^{(2,3,4,5)} - M_2^{(5)} L_{8LLH(7)}^{(1,2,3,4)} - M_{4a}^{(1,4,5)} L_{6LL(5)}^{(2,3)} \\ + \; & M_2^{(1)} L_2^{(4,5)} L_{6LL(5)}^{(2,3)} + M_2^{(5)} L_2^{(1,4)} L_{6LL(5)}^{(2,3)}. \end{aligned} \tag{A12}$$

The second-order vertex renormalization constants $L_2^{(1,4)}$ and $L_2^{(4,5)}$ appear in (A12) as reduced diagrams, which we called *implicit*, and used the full renormalization constant L_2 for them. Thus we define the finite amplitude by

$$\begin{aligned}\Delta M_{A3} &= M_{A3} - M_2^{(1)} L_{8LLJ(3)}^{(2,3,4,5)} - M_2^{(5)} L_{8LLH(7)}^{(1,2,3,4)} - M_{4a}^{(1,4,5)} L_{6LL(5)}^{(2,3)} \\ &+ M_2^{(1)} L_2^{(4,5)} L_{6LL(5)}^{(2,3)} + M_2^{(5)} L_2^{(1,4)} L_{6LL(5)}^{(2,3)}. \end{aligned} \tag{A13}$$

In other words, we have

$$a_{A3} = \Delta M_{A3}. \tag{A14}$$

Similar relation holds for a_{B3} and a_{C3}. Thus we have

$$\sum_{\alpha=A}^{C} a_{\alpha 3} = \sum_{\alpha=A}^{C} \Delta M_{\alpha 3}. \tag{A15}$$

4. *A4, B4, C4*

The diagram $A4$ has one self-energy subdiagram (2,3,4) and two vertex subdiagrams (2,3) and (3,4) as well as the l-l subdiagram (6,7,8,9). Thus the renormalized amplitude a_{A4} is given by

$$\begin{aligned}a_{A4} &= M_{A4} - M_{4b}^{(1,2,5)} L_{6LL(5)}^{(3,4)} - M_{4b}^{(1,4,5)} L_{6LL(5)}^{(2,3)} - M_2^{(1,5)} B_{8LLJ}^{(2,3,4)} - M_{2^*}^{(1,5)} \delta m_{8LLJ}^{(2,3,4)} \\ &+ M_2^{(1,5)} B_2^{(2)} L_{6LL(5)}^{(3,4)} + M_{2^*}^{(1,5)} \delta m_2^{(2)} L_{6LL(5)}^{(3,4)} \\ &+ M_2^{(1,5)} B_2^{(4)} L_{6LL(5)}^{(2,3)} + M_{2^*}^{(1,5)} \delta m_2^{(4)} L_{6LL(5)}^{(2,3)}. \end{aligned} \tag{A16}$$

We define the UV-finite amplitude $\Delta' M_{A4}$ by

$$\begin{aligned}\Delta' M_{A4} &= M_{A4} - M_{4b}^{(1,2,5)} L_{6LL(5)}^{(3,4)} - M_{4b}^{(1,4,5)} L_{6LL(5)}^{(2,3)} - M_2^{(1,5)} B_{8LLJ}^{(2,3,4)} - M_{2^*}^{(1,5)} \delta m_{8LLJ}^{(2,3,4)} \\ &+ M_2^{(1,5)} B_2^{(2)} L_{6LL(5)}^{(3,4)} + M_{2^*}^{(1,5)} \delta m_2^{(2)} L_{6LL(5)}^{(3,4)} \\ &+ M_2^{(1,5)} B_2^{(4)} L_{6LL(5)}^{(2,3)} + M_{2^*}^{(1,5)} \delta m_2^{(4)} L_{6LL(5)}^{(2,3)}, \end{aligned} \tag{A17}$$

where M_{2^*} is derived from M_2 by inserting a two-point vertex in the lepton line. Note that the renormalization constants B_2 and δm_2 arising from the self-energy subdiagrams {2;a} and {4;d} are subtracted as a whole without breaking them up into UV-divergent and UV-finite parts. This is consistent only if we use the full body of the renormalization constant B_{8LLJ}. Otherwise, IR-singular part of B_{8LLJ} and two B_2's do not cancel out each other. Substituting (A17) in (A16), we obtain

$$a_{A4} = \Delta' M_{A4}. \tag{A18}$$

The resulting a_{A4} is UV-finite but IR-divergent. Separating the IR divergence of $\Delta' M_{A4}$ from the subdiagram {1,5;e} by the I-operation, we can write

$$a_{A4} = \Delta M_{A4} + L_2^{\mathrm{R}}(M_{8LLJ}^{(2,3,4)} - 2L_{6LL(5)}M_2) = \Delta M_{A4} + L_2^{\mathrm{R}}\Delta M_{8LLJ}^{(2,3,4)}. \tag{A19}$$

Similarly we have

$$a_{B4} = \Delta M_{B4} + L_2^{\mathrm{R}}(M_{8LLL}^{(2,3,4)} - 2L_{6LL(3)}M_2) = \Delta M_{B4} + L_2^{\mathrm{R}}\Delta M_{8LLL}^{(2,3,4)}, \tag{A20}$$

and

$$a_{C4} = \Delta M_{C4} + L_2^{\mathrm{R}}(M_{8LLK}^{(2,3,4)} - 2L_{6LL(3)}M_2) = \Delta M_{C4} + L_2^{\mathrm{R}}\Delta M_{8LLK}^{(2,3,4)}. \tag{A21}$$

Adding up these three results we obtain

$$\sum_{\alpha=A}^{C} a_{\alpha 4} = \sum_{\alpha=A}^{C} \Delta M_{\alpha 4} + L_2^{\mathrm{R}}\Delta M_{8JKL}, \tag{A22}$$

noting that gauge invariance guarantees the vanishing of the sum $L_{6LL} \equiv L_{6LL(3)} + L_{6LL(4)} + L_{6LL(5)} = 0$.

We also developed an alternative method for separating UV-divergence from M_{A4}, in which a UV-finite amplitude is defined by

$$\begin{aligned}
\Delta'' M_{A4} \;=\; & M_{A4} - M_{4b}^{(1,2,5)}L_{6LL(5)}^{(3,4)} - M_{4b}^{(1,4,5)}L_{6LL(5)}^{(2,3)} - M_2^{(1,5)}B_{8LLJ}(E)^{(2,3,4)} - M_{2^*}^{(1,5)}\delta m_{8LLJ}^{(2,3,4)} \\
+ \; & M_2^{(1,5)}B_2^{(2)}(E)L_{6LL(5)}^{(3,4)} + M_{2^*}^{(1,5)}\delta m_2^{(2)}L_{6LL(5)}^{(3,4)} \\
+ \; & M_2^{(1,5)}B_2^{(4)}(E)L_{6LL(5)}^{(2,3)} + M_{2^*}^{(1,5)}\delta m_2^{(4)}L_{6LL(5)}^{(2,3)},
\end{aligned} \tag{A23}$$

where

$$\begin{aligned}
B_{8LLJ} \;&=\; B_{8LLJ}(E) + B_{8LLJ}(N), \\
B_2 \;&=\; B_2(E) + B_2(N).
\end{aligned} \tag{A24}$$

The $B(E)$ term of the wave-function renormalization constant comes from the derivative of the numerator of the self-energy diagram $\Sigma(p)$ with respect to the fermion momentum p, while the $B(N)$ term is the derivative of the denominator function V defined in (11). For the second-order case, we find $B_2(E) = B_2^{\mathrm{UV}}$ and $B_2(N) = B_2^{\mathrm{R}}$. The relationship to the fully subtracted $\Delta' M_{A4}$ is thus clear and we find

$$\begin{aligned}
\Delta' M_{A4} \;&=\; \Delta'' M_{A4} - M_2^{(1,5)}\Delta B_{8LLJ}^{(2,3,4)}, \\
\Delta B_{8LLJ} \;&\equiv\; B_{8LLJ}(N) - 2B_2^{\mathrm{R}}L_{6LL(5)}\ .
\end{aligned} \tag{A25}$$

The IR subtraction term used for $\Delta'' M_{A4}$ is the same one for $\Delta' M_{A4}$. As a check we evaluated both integrals numerically. The results are in good agreement within the uncertainty of VEGAS integration.

5. *A5, B5, C5*

The diagram $A5$ has a self-energy subdiagram (2) and two vertex subdiagrams (1,2,3,4) and (4,5) besides the l-l subdiagram (6,7,8,9). The subdiagram (2) is the second-order self-energy diagram which contributes to the renormalization constants B_2 and δm_2. Taking this into account we can write the renormalized amplitude a_{A5} as

$$\begin{aligned} a_{A5} &= M_{A5} - L^{(4,5)}_{6LL(5)} M^{(1,2,3)}_{4b} - L^{(1,2,3,4)}_{8LLI(7)} M^{(5)}_2 - B^{(2)}_2 M^{(1,3,4,5)}_{8LLJ} - \delta m^{(2)}_2 M^{(1,3,4,5)}_{8LLJ^*} \\ &+ B^{(2)}_2 L^{(1,3,4)}_{6LL(5)} M^{(5)}_2 + \delta m^{(2)}_2 L^{(1,3,4)}_{6LL^*(5)} M^{(5)}_2 \\ &+ B^{(2)}_2 L^{(4,5)}_{6LL(5)} M^{(1,3)}_2 + \delta m^{(2)}_2 L^{(4,5)}_{6LL(5)} M^{(1,3)}_{2^*}. \end{aligned} \tag{A26}$$

Applying the K_2-operation to the self-energy subdiagram (2), we obtain

$$\begin{aligned} \Delta M_{A5} &= M_{A5} - L^{(4,5)}_{6LL(5)} M^{(1,2,3)}_{4b} - L^{(1,2,3,4)}_{8LLI(7)} M^{(5)}_2 - B^{(2)UV}_2 M^{(1,3,4,5)}_{8LLJ} - \delta m^{(2)}_2 M^{(1,3,4,5)}_{8LLJ^*} \\ &+ B^{(2)UV}_2 L^{(1,3,4)}_{6LL(5)} M^{(5)}_2 + \delta m^{(2)}_2 L^{(1,3,4)}_{6LL^*(5)} M^{(5)}_2 \\ &+ B^{(2)UV}_2 L^{(4,5)}_{6LL(5)} M^{(1,3)}_2 + \delta m^{(2)}_2 L^{(4,5)}_{6LL(5)} M^{(1,3)}_{2^*}. \end{aligned} \tag{A27}$$

Note that the K_2-operation yields the whole mass-renormalization constant δm_2. Substituting (A27) in (A26), we obtain

$$\begin{aligned} a_{A5} &= \Delta M_{A5} - B^{\mathrm{R}}_2 M^{(1,3,4,5)}_{8LLJ} + B^{\mathrm{R}}_2 L^{(1,3,4)}_{6LL(5)} M^{(5)}_2 + B^{\mathrm{R}}_2 L^{(4,5)}_{6LL(5)} M^{(1,3)}_2 \\ &= \Delta M_{A5} - B^{\mathrm{R}}_2 \Delta M_{8LLJ} \end{aligned} \tag{A28}$$

where $B^{\mathrm{R}}_2 = B_2 - B^{UV}_2$. Similar consideration for the diagrams B5 and C5 yields

$$\begin{aligned} a_{B5} &= \Delta M_{B5} - B^{\mathrm{R}}_2 M^{(1,3,4,5)}_{8LLL} + B^{\mathrm{R}}_2 L^{(1,3,4)}_{6LL(3)} M^{(5)}_2 + B^{\mathrm{R}}_2 L^{(4,5)}_{6LL(3)} M^{(1,3)}_2 \\ &= \Delta M_{B5} - B^{\mathrm{R}}_2 \Delta M_{8LLL} \end{aligned} \tag{A29}$$

$$\begin{aligned} a_{C5} &= \Delta M_{C5} - B^{\mathrm{R}}_2 M^{(1,3,4,5)}_{8LLK} + B^{\mathrm{R}}_2 L^{(1,3,4)}_{6LL(3)} M^{(5)}_2 + B^{\mathrm{R}}_2 L^{(4,5)}_{6LL(3)} M^{(1,3)}_2 \\ &= \Delta M_{C5} - B^{\mathrm{R}}_2 \Delta M_{8LLK}. \end{aligned} \tag{A30}$$

Adding up these results, we obtain

$$\sum_{\alpha=A}^{C} a_{\alpha 5} = \sum_{\alpha=A}^{C} \Delta M_{\alpha 5} - B^{\mathrm{R}}_2 \Delta M_{8JKL}. \tag{A31}$$

6. *A6, B6, C6*

The diagram $A6$ has UV-divergent subdiagrams $(2,3),(1,2,3,4),(2,3,4,5)$, besides $(6,7,8,9)$, and the corresponding forest structure. Thus the renormalized amplitude a_{A6} can be written as

$$\begin{aligned} a_{A6} &= M_{A6} - L_2^{(2,3)} M_{8LLJ}^{(1,4,5)} - L_{8LLE(7)}^{(1,2,3,4)} M_2^{(5)} - L_{8LLF(7)}^{(2,3,4,5)} M_2^{(1)} \\ &+ L_2^{(2,3)} L_{6LL(5)}^{(4,5)} M_2^{(1)} + L_2^{(2,3)} L_{6LL(5)}^{(1,4)} M_2^{(5)}. \end{aligned} \tag{A32}$$

Applying the K_{23}-operation on M_{A6}, we can define the UV-finite quantity ΔM_{A6} as

$$\begin{aligned} \Delta M_{A6} &= M_{A6} - L_2^{UV(2,3)} M_{8LLJ}^{(1,4,5)} - L_{8LLE(7)}^{(1,2,3,4)} M_2^{(5)} - L_{8LLF(7)}^{(2,3,4,5)} M_2^{(1)} \\ &+ L_2^{UV(2,3)} L_{6LL(5)}^{(4,5)} M_2^{(1)} + L_2^{UV(2,3)} L_{6LL(5)}^{(1,4)} M_2^{(5)}. \end{aligned} \tag{A33}$$

Substituting (A33) in (A32), we obtain

$$\begin{aligned} a_{A6} &= \Delta M_{A6} - L_2^{\mathrm{R}} M_{8LLJ}^{(1,4,5)} + L_2^{\mathrm{R}} L_{6LL(5)}^{(4,5)} M_2 + L_2^{\mathrm{R}} L_{6LL(5)}^{(1,4)} M_2 \\ &= \Delta M_{A6} - L_2^{\mathrm{R}} \Delta M_{8LLJ}. \end{aligned} \tag{A34}$$

Similar consideration for the diagrams $B6$ and $C6$ yields

$$\begin{aligned} a_{B6} &= \Delta M_{B6} - L_2^{\mathrm{R}} M_{8LLL}^{(1,4,5)} + L_2^{\mathrm{R}} L_{6LL(3)}^{(4,5)} M_2 + L_2^{\mathrm{R}} L_{6LL(3)}^{(1,4)} M_2 \\ &= \Delta M_{B6} - L_2^{\mathrm{R}} \Delta M_{8LLL}, \end{aligned} \tag{A35}$$

and

$$\begin{aligned} a_{C6} &= \Delta M_{C6} - L_2^{\mathrm{R}} M_{8LLK}^{(1,4,5)} + L_2^{\mathrm{R}} L_{6LL(3)}^{(4,5)} M_2 + L_2^{\mathrm{R}} L_{6LL(3)}^{(1,4)} M_2 \\ &= \Delta M_{C6} - L_2^{\mathrm{R}} \Delta M_{8LLK}. \end{aligned} \tag{A36}$$

From (A34), (A35), and (A36), we obtain

$$\sum_{\alpha=A}^{C} a_{\alpha 6} = \sum_{\alpha=A}^{C} \Delta M_{\alpha 6} - L_2^{\mathrm{R}} \Delta M_{8JKL}. \tag{A37}$$

7. *A7, B7, C7*

The diagram $A7$ has two vertex subdiagrams (1,2,3,4) and (2,3,4,5), besides the l-l subdiagram (6,7,8,9). Thus the renormalized amplitude a_{A7} can be written as

$$a_{A7} = M_{A7} - L_{8LLG(7)}^{(1,2,3,4)} M_2^{(5)} - L_{8LLG(7)}^{(2,3,4,5)} M_2^{(1)}. \tag{A38}$$

We define the UV-finite quantity ΔM_{A7} by

$$\Delta M_{A7} \; = \; M_{A7} - L^{(1,2,3,4)}_{8LLG(7)} M_2^{(5)} - L^{(2,3,4,5)}_{8LLG(7)} M_2^{(1)}, \tag{A39}$$

where $L_{8LLG(7)}$ is not decomposed into UV-divergent and UV-finite parts. Thus we have

$$a_{A7} = \Delta M_{A7}. \tag{A40}$$

Similar relation holds for a_{B7} and a_{C7}. Thus we have

$$\sum_{\alpha=A}^{C} a_{\alpha 7} = \sum_{\alpha=A}^{C} \Delta M_{\alpha 7}. \tag{A41}$$

8. *A8, B8, C8*

The diagram $A8$ has a self-energy subdiagram (3) and two vertex subdiagrams (1,2,3,4) and (2,3,4,5), besides the l-l subdiagram (6,7,8,9). Thus, its renormalization structure is similar to that of the diagram $A5$:

$$\begin{aligned} a_{A8} \; &= \; M_{A8} - L^{(1,2,3,4)}_{8LLI(7)} M_2^{(5)} - L^{(2,3,4,5)}_{8LLI(7)} M_2^{(1)} - B_2^{(3)} M^{(1,2,4,5)}_{8LLJ} - \delta m_2^{(3)} M^{(1,2,4,5)}_{8LLJ^*} \\ &+ \; B_2^{(3)} L^{(1,2,4)}_{6LL(5)} M_2^{(5)} + \delta m_2^{(3)} L^{(1,2,4)}_{6LL^*(5)} M_2^{(5)} \\ &+ \; B_2^{(3)} L^{(2,4,5)}_{6LL(5)} M_2^{(1)} + \delta m_2^{(3)} L^{(2,4,5)}_{6LL^*(5)} M_2^{(1)}. \end{aligned} \tag{A42}$$

Applying the K_3-operation to the self-energy subdiagram (3), we obtain

$$\begin{aligned} \Delta M_{A8} \; &= \; M_{A8} - L^{(1,2,3,4)}_{8LLI(7)} M_2^{(5)} - L^{(2,3,4,5)}_{8LLI(7)} M_2^{(1)} - B_2^{(3)UV} M^{(1,2,4,5)}_{8LLJ} - \delta m_2^{(3)} M^{(1,2,4,5)}_{8LLJ^*} \\ &+ \; B_2^{(3)UV} L^{(1,2,4)}_{6LL(5)} M_2^{(5)} + \delta m_2^{(3)} L^{(1,2,4)}_{6LL^*(5)} M_2^{(5)} \\ &+ \; B_2^{(3)UV} L^{(2,4,5)}_{6LL(5)} M_2^{(1)} + \delta m_2^{(3)} L^{(2,4,5)}_{6LL^*(5)} M_2^{(1)}. \end{aligned} \tag{A43}$$

Substituting (A43) in (A42), we obtain

$$\begin{aligned} a_{A8} \; &= \; \Delta M_{A8} - B_2^{\mathrm{R}} M^{(1,3,4,5)}_{8LLJ} + B_2^{\mathrm{R}} L^{(1,2,4)}_{6LL(5)} \Delta M_2^{(5)} + B_2^{\mathrm{R}} L^{(2,4,5)}_{6LL(5)} \Delta M_2^{(1)} \\ &= \; \Delta M_{A8} - B_2^{\mathrm{R}} \Delta M^{(1,3,4,5)}_{8LLJ}. \end{aligned} \tag{A44}$$

Applying the same consideration to the diagrams $B8$ and $C8$, and adding them to (A44), we obtain

$$\sum_{\alpha=A}^{C} a_{\alpha 8} = \sum_{\alpha=A}^{C} \Delta M_{\alpha 8} - B_2^{\mathrm{R}} \Delta M_{8JKL}. \tag{A45}$$

9. Sum

Taking into account that integrals for diagrams such as $A1$ actually represent $2 \times 2 \times 5$ vertex diagrams, the sum of all diagrams of Set III(c) can be written as

$$A_1^{(10)}[\text{Set III(c)}^{(l_1 l_2)}] = \sum_{\alpha=A}^{C} \sum_{i=1}^{8} \eta_i \Delta M_{\alpha i}^{(l_1 l_2)} - 3\Delta LB_2 \Delta M_{8JKL}^{(l_1 l_2)}, \tag{A46}$$

where l_1 refers to the open lepton line and l_2 refers to the closed lepton line. $\Delta LB_2 \equiv L_2^{\mathrm{R}} + B_2^{\mathrm{R}}$, and $\eta_i = 2$ for $i = 4, 7, 8$, $\eta_i = 4$ for $i = 1, 2, 3, 5, 6$.

---

[1] D. Hanneke, S. Fogwell, and G. Gabrielse, Phys. Rev. Lett. **100**, 120801 (2008).

[2] D. Hanneke, S. Fogwell Hoogerheide, and G. Gabrielse, Phys. Rev. A **83**, 052122 (2011).

[3] T. Kinoshita and M. Nio, Phys. Rev. D **73**, 053007 (2006).

[4] T. Aoyama, M. Hayakawa, T. Kinoshita, and M. Nio, Phys. Rev. Lett. **99**, 110406 (2007).

[5] T. Aoyama, M. Hayakawa, T. Kinoshita, and M. Nio, Phys. Rev. D **77**, 053012 (2008).

[6] M. Davier, A. Hoecker, B. Malaescu, and Z. Zhang, Eur. Phys. J. **C71**, 1515 (2011).

[7] K. Hagiwara, R. Liao, A. D. Martin, D. Nomura, and T. Teubner, J. Phys. G **38**, 085003 (2011).

[8] B. Krause, Phys. Lett. **B390**, 392 (1997).

[9] K. Melnikov and A. Vainshtein, Phys. Rev. D **70**, 113006 (2004).

[10] J. Bijnens and J. Prades, Mod. Phys. Lett. **A22**, 767 (2007).

[11] J. Prades, E. de Rafael, and A. Vainshtein, in *Lepton dipole moments*, edited by L. B. Roberts and W. J. Marciano (World Scientific, Singapore, 2009), pp. 303–317.

[12] A. Nyffeler, Phys. Rev. D **79**, 073012 (2009).

[13] A. Czarnecki, B. Krause, and W. J. Marciano, Phys. Rev. Lett. **76**, 3267 (1996).

[14] M. Knecht, S. Peris, M. Perrottet, and E. De Rafael, JHEP **11**, 003 (2002).

[15] A. Czarnecki, W. J. Marciano, and A. Vainshtein, Phys. Rev. D **67**, 073006 (2003), **73**, 119901(E) (2006).

[16] R. Bouchendira, P. Clade, S. Guellati-Khelifa, F. Nez, and F. Biraben, Phys.Rev.Lett. **106**, 080801 (2011).

[17] P. J. Mohr, B. N. Taylor, and D. B. Newell, Rev. Mod. Phys. **80**, 633 (2008).

[18] T. Kinoshita and M. Nio, Phys. Rev. D **70**, 113001 (2004).

[19] T. Aoyama, M. Hayakawa, T. Kinoshita, and M. Nio, Nucl. Phys. **B740**, 138 (2006).

[20] T. Aoyama, M. Hayakawa, T. Kinoshita, and M. Nio, Nucl. Phys. **B796**, 184 (2008).

[21] T. Aoyama, M. Hayakawa, T. Kinoshita, M. Nio, and N. Watanabe, Phys. Rev. D **78**, 053005 (2008).

[22] T. Aoyama, M. Hayakawa, T. Kinoshita, and M. Nio, Phys. Rev. D **78**, 113006 (2008).

[23] T. Aoyama, K. Asano, M. Hayakawa, T. Kinoshita, M. Nio, and N. Watanabe, Phys. Rev. D **81**, 053009 (2010).

[24] T. Aoyama, M. Hayakawa, T. Kinoshita, and M. Nio, Phys.Rev.D **82**, 113004 (2010).

[25] T. Aoyama, M. Hayakawa, T. Kinoshita, and M. Nio, Phys.Rev.D **83**, 053003 (2011).

[26] T. Aoyama, M. Hayakawa, T. Kinoshita, and M. Nio, Phys.Rev.D **83**, 053002 (2011).

[27] T. Aoyama, M. Hayakawa, T. Kinoshita, and M. Nio, Phys.Rev.D **84**, 053003 (2011).

[28] T. Aoyama, M. Hayakawa, T. Kinoshita, and M. Nio, arXiv:1110.2826 [hep-ph], to appear in PRD.

[29] S. Laporta, Phys. Lett. **B328**, 522 (1994).

[30] J.-P. Aguilar, E. de Rafael, and D. Greynat, Phys.Rev.D **77**, 093010 (2008).

[31] T. Kinoshita and W. B. Lindquist, Phys. Rev. D **39**, 2407 (1989).

[32] T. Kinoshita and M. Nio, Phys. Rev. Lett. **90**, 021803 (2003).

[33] J. A. M. Vermaseren, math-ph/0010025.

[34] T. Kinoshita, in *Quantum electrodynamics*, edited by T. Kinoshita (World Scientific, Singapore, 1990), pp. 218–321, (Advanced series on directions in high energy physics, 7).

[35] W. Zimmermann, Commun. Math. Phys. **15**, 208 (1969).

[36] G. P. Lepage, J. Comput. Phys. **27**, 192 (1978).